Bol. Soc. Paran. Mat.
©SPM – E-ISSN-2175-1188
SPM: www.spm.uem.br/bspm

(3s.) **v. 2025 (43)** : 1–14.
ISSN-0037-8712
doi:10.5269/bspm.77629

Image Denoising via Optimal Control of the Diffusivity Function in a PDE-constrained problem

Kawtar Lehrizi, Omar Gouasnouane, Noureddine Moussaid and Anouar Ben-Loghfyry*

ABSTRACT: In this paper, we suggest a new picture denoising model for PDE-constrained problem that is based on the popular Perona-Malik model. We present a novel method based on the optimal control of the diffusivity function to overcome the staircasing effect and contrast loss, two intrinsic drawbacks of the Perona-Malik equation. Through adaptively controlling the diffusion process, our model successfully improves noise reduction while maintaining important image characteristics. Comparisons with some models show how much better our method is at preserving structural features and improving denoising performance.

Key Words: Image denoising, Perona-Malik model, PDE-constrained, optimal control, diffusivity function.

1. Introduction

Image processing is a method that aims to enhance the quality of an image, to obtain an enhanced image, or to extract useful information from it, with a view to adjusting the obtained image for further processing or analysis (see [2,20]). Image processing encompasses a wide range of domains, including, but not limited to, image denoising [9,10,11,12] (the primary focus of this paper), image super-resolution [5,6,8], image recognition [15], image encryption [16] and image inpainting [13,14]. Image denoising is a fundamental problem in image processing, where the goal is to recover a clean image $u : \Omega \subset \mathbb{R}^2 \to \mathbb{R}$ from a corrupted observation u_0, generally degraded by additive noise (see [35,17]). Mathematically, the observed image is modeled as:

$$u_0(x) = u(x) + \eta(x), \qquad x \in \Omega. \tag{1.1}$$

Where η is a random noise term, frequently assumed to be white Gaussian [18]. The challenge lies in constructing a regularization strategy that suppresses noise while preserving meaningful structures such as edges and textures [19]. A natural and early approach to image denoising stems from the linear heat equation [1], which models the image evolution as a diffusion process:

$$\frac{\partial u}{\partial t} = \Delta u, \quad u(x,0) = u_0(x), \qquad x \in \Omega. \tag{1.2}$$

With homogeneous Neumann boundary conditions. This equation corresponds to the gradient descent of the Dirichlet energy functional:

$$E(u) = \int_\Omega \frac{1}{2}|\nabla u|^2 \, dx. \tag{1.3}$$

Which promotes smooth solutions by penalizing gradient magnitude [1]. However, this isotropic smoothing indiscriminately blurs all regions, including edges, which are critical for human perception and subsequent processing.
To address this limitation, Perona and Malik (1990) proposed an anisotropic diffusion model (see [21,22]) of the form:

$$\frac{\partial u}{\partial t} = \nabla \cdot (g(|\nabla u|)\nabla u), \quad u(x,0) = u_0(x). \tag{1.4}$$

Where the diffusivity function $g : \mathbb{R}^+ \to \mathbb{R}^+$ is chosen to be decreasing, such that the diffusion slows down across edges (high gradient) and accelerates in flat regions (low gradient).
Two typical examples are:

$$g(s) = \frac{1}{1 + (s/K)^2}, \quad \text{and} \quad g(s) = \exp\left(-\left(\frac{s}{K}\right)^2\right), \tag{1.5}$$

* Corresponding author.
2010 *Mathematics Subject Classification:* 35B40, 35L70.
Submitted July 02, 2025. Published September 17, 2025

where $K > 0$ is an edge-thresholding parameter. This formulation corresponds to a nonlinear diffusion process, which can be formally seen as the gradient flow of the energy:

$$E(u) = \int_\Omega \phi(|\nabla u|)\, dx, \quad \text{with} \quad \phi'(|\nabla u|) = |\nabla u| \cdot g(|\nabla u|). \tag{1.6}$$

Despite its intuitive appeal, the Perona-Malik equation is ill-posed due to the non-monotonicity of g, which can result in backward diffusion and loss of well-posedness in the PDE sense. To ensure stability and well-posedness, variational methods have been introduced. A classical approach is the Tikhonov regularization, which seeks the minimizer of the functional:

$$J(u) = \underbrace{\frac{1}{2}\|u - u_0\|^2_{L^2(\Omega)}}_{\text{Fidelity term}} + \underbrace{\alpha\|\nabla u\|^2_{L^2(\Omega)}}_{\text{Regularization term}}. \tag{1.7}$$

Where $\alpha > 0$ balances fidelity to data and smoothness. The associated Euler-Lagrange equation leads back to a stationary heat equation. However, this model still suffers from over-smoothing and poor edge preservation [24]. In contrast, the Total Variation (TV) model proposed by Rudin, Osher, and Fatemi (see [19]) defines the regularization through the total variation norm:

$$J(u) = \frac{1}{2}\|u - u_0\|^2_{L^2(\Omega)} + \lambda \int_\Omega |\nabla u|\, dx, \tag{1.8}$$

which allows for piecewise smooth results and discontinuous edges, making it particularly effective in preserving image structures. However, the non-differentiability of the TV term poses numerical and analytical challenges, especially in large-scale or real-time applications [7]. In this study, we return to the Perona-Malik paradigm and propose to address its limitations via optimal control theory. Instead of fixing the diffusivity function g, we treat it as a control function to be optimized. Specifically, we formulate an optimal control problem in which the state equation is the Perona-Malik model:

$$\frac{\partial u}{\partial t} = \nabla \cdot (g(x,t,|\nabla u|)\nabla u), \quad u(x,0) = u_0(x), \tag{1.9}$$

and the objective is to minimize a cost functional of the form:

$$J(g,u) = \frac{1}{2}\int_\Omega |u(x,T) - u_{\text{ref}}(x)|^2\, dx + \beta \int_0^T \int_\Omega \Psi(g(x,t,s))\, dx\, dt, \tag{1.10}$$

where u_{ref} is a reference clean image, Ψ is a regularization term enforcing desirable properties on g, and $\beta > 0$ balances data fidelity and regularity of the control. The control g is sought in an admissible set $\mathcal{G}_{ad}$ ensuring monotonicity and positivity constraints to guarantee well-posedness of the state equation. This formulation allows for a data-driven, adaptive design of the diffusivity function, optimized with respect to image quality, while retaining the physical interpretability of anisotropic diffusion. The resulting framework bridges the gap between PDE-based models and modern variational techniques, opening new directions for robust, edge-preserving image restoration (see [25,26]).

2. Proposed model And Well-posedness

In this section, we offer a condensed overview of a designed denoising model, which merges the contributions of Perona and Malik with the principles of optimal control. Next, we propose a succinct mathematical framework to address the problem at hand. Finally, the proof of the existence and uniqueness of a solution to the suggested model in a suitable framework reinforces our major theoretical conclusions.

2.1. Statement of the proposed model

we consider the following controlled problem:
We are looking for a function $u(x,t)$ defined on a domain $\Omega \subset \mathbb{R}^n$ and on a time interval $[0,T]$, which constitutes the solution of the system :

$$(\mathcal{P})\begin{cases}\frac{\partial u}{\partial t}-\nabla\cdot(q(x)\nabla u(x))=0, & x\in\Omega, \quad t\in[0,T]\\ u(x,0)=f, & x\in\Omega\\ \frac{\partial u}{\partial n}=0, & t\in[0,T] \quad \text{and} \quad x\in\partial\Omega.\end{cases} \tag{2.1}$$

where $q(x)$ is a control function defined on the domain $\Omega\subset\mathbb{R}^n$, t the time, u the desired image, f is the initial image, and the homogeneous Neumann condition reflects flux conservation at the boundary. The objective is to define the control function $q(x)$ which is used to minimize the following cost function :

$$J(u,q)=\frac{1}{2}\int_0^T\int_\Omega(u(x,t)-f(x))^2dxdt+\alpha\int_0^T\int_\Omega R(u(x,t),q)dxdt. \tag{2.2}$$

Where the first term measures the deviation between the state of the system and the initial image, while the second term is a regularization controlled by a parameter $\alpha>0$.
The function $R(u,q)$ can be defined in this way:

$$R(u,q)=\frac{1}{2}\int_\Omega|\nabla u(x)|^2dx. \tag{2.3}$$

To penalize excessive values of the control function. Thus, the task is to reduce the function J(u,q) while respecting the condition that u must be a solution of the previously mentioned system.

2.2. Solvability of the proposed model

To study the solvency of our model, we begin by :

Step 1: Variational Formulation . In this step, we aim to give the variational formulation of the model (1).
As a first step, let ϕ be the test function such that :

$$\phi\in H_0^1(\Omega)$$

The model terms are then multiplied by ϕ, giving :

$$\int_0^T\int_\Omega\frac{\partial u}{\partial t}\phi dxdt-\int_0^T\int_\Omega\nabla\cdot(q(x)\nabla u(x,t))dxdt=0. \tag{2.4}$$

Using Green's first formula, we get :

$$\int_\Omega\frac{\partial u}{\partial t}\phi dx=\int_{\partial\Omega}u(t,x)\frac{\partial\phi}{\partial\eta}\,d\nu-\int_\Omega u(t,x)\frac{\partial\phi}{\partial t}\,dx-\int_\Omega u(t,x)\frac{\partial\phi}{\partial\eta}dx \tag{2.5}$$

and

$$\int_\Omega\nabla\cdot(q(x)\nabla u(x,t))dx=\int_{\partial\Omega}q(x)\nabla u(t,x)\frac{\partial\phi}{\partial\eta}\,d\nu-\int_\Omega u(t,x)\frac{\partial\phi}{\partial t}\,dx-\int_\Omega q(x)\nabla u(t,x)\frac{\partial\phi}{\partial t}dx \tag{2.6}$$

Then, from (4) and (5) the bilinear form is :

$$a(u,\phi)=<\dot{u},\phi>+\int_\Omega q(x)(\nabla u.\nabla\phi)dx. \tag{2.7}$$

Step 2: Lagrangian Formula .In this paragraph, we'll provides the Lagrangian corresponding to control problem (1) as follows :

$$\mathcal{L}(u,\phi,q)=J(u,q)-\int_0^T<\dot{u},\phi>dt-\int_0^T\int_\Omega q(x)(\nabla u.\nabla\phi)dtdx. \tag{2.8}$$

Where the functional $J(u,q)$ represents the cost to be minimized.

Step 3: Adjoint System . To obtain the adjoint system, we derive the Lagrangian with respect to state u in the direction of a regular test function $\omega(x,t)$. Application of integrations by parts gives :

$$\frac{\partial \mathcal{L}}{\partial u} = J(u,q) + \int_0^T \langle u, \dot{\phi} \rangle \, dt + (u(0), \phi(0)) - (u(T), \phi(T)) - \int_0^T \int_\Omega q(x)(\nabla u \cdot \nabla \phi) dt dx.$$

By making this directional derivative zero for any permissible variation ω, i.e. $(\frac{\partial \mathcal{L}}{\partial u}, \omega) = 0$.
Therefore

$$-\int_0^T \langle \omega, \dot{\phi} \rangle dt - (\omega(T), \phi(T)) + \int_0^T \int_\Omega \nabla(q(x)\nabla\omega) dx dt \quad + \int_0^T \int_\Omega (u-f)\omega dx dt + \alpha \int_0^T \int_\Omega \frac{\partial R}{\partial u}(u,q)\omega \, dx \, dt = 0$$

The following adjoint system can be deduced:

$$\begin{cases} -\frac{\partial p}{\partial t} + \nabla \cdot (q(x)\nabla p) = -(u-f) - \alpha \frac{\partial R}{\partial u}(u,q), & \Omega \times [0,T], \\ p(T) = 0, & \text{in} \quad \Omega, \\ \frac{\partial p}{\partial \eta} = 0, & \text{in } \partial\Omega \times [0,T]. \end{cases} \tag{2.9}$$

Where η denotes the normal direction outside the boundary $\partial\Omega$, $\alpha \frac{\partial R}{\partial u}(u,q)$ indicates the derivative with respect to the regularization state and $P(x,t)$ represents the adjoint variable introduced for the satisfaction of the first-order optimality conditions.

Step 4: Optimality conditions .In order to obtain the optimality conditions for control q, we begin by deriving the cost functional J with respect to q using the Lagrangian $\mathcal{L}(u,\phi,q)$. This gives :

$$\frac{\partial J}{\partial q} = \frac{\partial \mathcal{L}}{\partial q}. \tag{2.10}$$

Then, for any admissible variation δq, the following expression is obtained:

$$\left(\frac{\partial J}{\partial q}, \delta q\right) = \int_0^T \int_\Omega \delta q \, (\nabla u \cdot \nabla p) \, dx \, dt + \alpha \int_0^T \int_\Omega \frac{\partial R}{\partial q}(u,q) \, \delta q \, dx \, dt.$$

The gradient of J with respect to q can then be expressed as :

$$\frac{\partial J}{\partial q} = \nabla u \cdot \nabla p + \alpha \frac{\partial R}{\partial q}(u,q). \tag{2.11}$$

The optimality condition for q is then given by the cancellation of the gradient, which leads to the final optimality condition :

$$\nabla u \cdot \nabla p + \alpha \frac{\partial R}{\partial q}(u,q) = 0. \tag{2.12}$$

This condition states that the optimality of control q would be relative not only to state u and the adjoint state p, but also to the regularization R. It also plays a strategic role in solving the optimal control problem, enabling us to link, or associate, the evolution of the system state with the optimal control strategy to be adopted.

Existence result :
Consider $\Omega \subset \mathbb{R}^n$ as a bounded domain with a Lipschitzian boundary, and set a final time $T > 0$.
We consider the following parabolic equation with homogeneous Neumann conditions :

$$\begin{cases} \frac{\partial u}{\partial t} - \nabla \cdot (q(x)\nabla u) = 0 & \text{in } \Omega \times (0,T), \\ \frac{\partial u}{\partial \eta} = 0 & \text{on } \partial\Omega \times (0,T), \\ u(x,0) = f & \text{in } \Omega. \end{cases} \tag{2.13}$$

Where $f \in L^2(\Omega)$ is the initial condition, and $q \in Q_{\text{ad}} \subset L^\infty(\Omega)$ is a diffusion coefficient that plays the role of the control.

The admissible set is formulated as follows:

$$Q_{\text{ad}} := \{q \in L^\infty(\Omega) : q(x) \geq q_0 > 0 \text{ p.p. on } \Omega\}. \tag{2.14}$$

Which ensures the coercivity of the associated elliptic operator.

Existence and uniqueness of the state solution.

Under the assumptions made, there is a unique weak solution given by

$$u \in L^2(0,T;H_0^1(\Omega)) \cap H^1(0,T;H^{-1}(\Omega)), \tag{2.15}$$

for the state problem.

The presence and uniqueness of the weak solution of the state problem follows from traditional theorems relating to linear parabolic equations (see [27,28]). The assumption $q(x) \geq q_0 > 0$ ensures the coercivity of the elliptic operator $-\nabla \cdot (q(x)\nabla u)$, thereby guaranteeing the energy stability of the problem. Furthermore, in the homogeneous context where the second term is zero (i.e., $f(u,q) = 0$), the study is facilitated: you can directly use a Galerkin method, develop a series of approximate solutions, formulate a priori estimates, and then access the limit via compactness. This establishes the existence of a weak solution in the functional context $L^2(0,T;H_0^1(\Omega)) \cap H^1(0,T;H^{-1}(\Omega))$, and the uniqueness follows from the linearity of the problem.

Optimal control problem.

The following objective functional is to be minimized:

$$J(q) := \frac{1}{2}\int_0^T \|u(t) - u_d(t)\|^2_{L^2(\Omega)} dt + \frac{\alpha}{2}\|q\|^2_{L^2(\Omega)}, \tag{2.16}$$

where $u_d \in L^2(0,T;L^2(\Omega))$ represents the desired state, and $\alpha > 0$ is a regularization parameter.

Existence of optimal control.

The set Q_{ad} is both closed, convex and bounded in the space $L^2(\Omega)$, making it a weakly compact set. The application $q \mapsto u(q)$ has weak continuity from $L^2(\Omega)$ to $L^2(0,T;L^2(\Omega))$, due to the stability of parabolic solutions. In addition, the function J is weakly semi-continuous decreasing in $L^2(\Omega)$, since it consists of norms and scalar products.

According to the Weierstrass theorem in Banach spaces ([29]), an optimal control $\bar{q} \in Q_{\text{ad}}$ therefore exists such that

$$J(\bar{q}) = \min_{q \in Q_{\text{ad}}} J(q). \tag{2.17}$$

3. Discretization (Model Scheme)

In this section, we start by introducing a discrete form of our proposed model:

3.1. Discret Model

In order to introduce a discretization of Equation (1), we first present the finite difference discretization of the fractional derivative.

We define a spatial partition of the image domain Ω. Let u be an image of size $N \times M$ defined on Ω. We denote $u_{i,j}$ the value of the gray level at the pixel (i,j), for all $i = 1,\ldots,N$ and $j = 1,\ldots,M$.

For the discretization of $\nabla \cdot (q(x)\nabla u)$, We can rewrite :

$$\nabla \cdot (q(x)\nabla u) = \frac{\partial}{\partial x}\left(q(x)\frac{\partial u}{\partial x}\right) + \frac{\partial}{\partial y}\left(q(x)\frac{\partial u}{\partial y}\right). \tag{3.1}$$

Gradient discretization of u

The first step is to approximately calculate the derivatives of u(x). For this, we use centered finite

differences.
The derivative at x (centered difference)

$$\frac{\partial u}{\partial x}(x_i, y_j) \approx \frac{u_{i+1,j} - u_{i-1,j}}{2h}. \tag{3.2}$$

The derivative at y (centered difference)

$$\frac{\partial u}{\partial y}(x_i, y_j) \approx \frac{u_{i,j+1} - u_{i,j-1}}{2h}. \tag{3.3}$$

Discretization of the $q(x)\nabla u$ term
The product $q(x)\nabla u$ is discretized by calculating the flows along each of the x and y axes. Since $q(x)$ is a function of position, we'll approximate it in the midpoints between neighboring pixels:
In the x direction, we estimate $q(x)$ at the midpoint between i and $i+1$, then use the centered difference

$$\left(q(x)\frac{\partial u}{\partial x}\right)_{i,j} \approx \frac{1}{h}\left[q_{i+\frac{1}{2},j}\left(u_{i+1,j} - u_{i,j}\right) - q_{i-\frac{1}{2},j}\left(u_{i,j} - u_{i-1,j}\right)\right]. \tag{3.4}$$

Similarly, in the $y$direction, $q(x)$ is estimated at the center point between j and $j+1$

$$\left(q(x)\frac{\partial u}{\partial y}\right)_{i,j} \approx \frac{1}{h}\left[q_{i,j+\frac{1}{2}}\left(u_{i,j+1} - u_{i,j}\right) - q_{i,j-\frac{1}{2}}\left(u_{i,j} - u_{i,j-1}\right)\right]. \tag{3.5}$$

The full discretized expression for the divergence term $\nabla \cdot (q(x)\nabla u)$ is therefore as follows:

$$\nabla\cdot(q(x)\nabla u)_{i,j} \approx \frac{1}{h^2}\left[q_{i+\frac{1}{2},j}\left(u_{i+1,j} - u_{i,j}\right) - q_{i-\frac{1}{2},j}\left(u_{i,j} - u_{i-1,j}\right)\right] + \frac{1}{h^2}\left[q_{i,j+\frac{1}{2}}\left(u_{i,j+1} - u_{i,j}\right) - q_{i,j-\frac{1}{2}}\left(u_{i,j} - u_{i,j-1}\right)\right]. \tag{3.6}$$

This discretization makes it possible to maintain the physical characteristics of the model while evaluating changes in the image under the influence of the $q(x)$ control.

We start with the time discretization of the problem, to approximate the time derivative, we employ the implicit Euler scheme (the backward Euler method), which is known for its unconditional stability.The time derivative of $u(x,t)$ is discretized as follows:

$$\frac{\partial u}{\partial t}(x_i, y_j, t^n) \approx \frac{u_{i,j}^{n+1} - u_{i,j}^{n}}{\Delta t}. \tag{3.7}$$

where $u_{i,j}^{n+1}$ denotes the value of $u(x_i, y_j)$ at time t^{n+1}, and $u_{i,j}^{n}$ denotes the value at time t^n.

Rewriting this expression yields the following update equation:

$$u_{i,j}^{n+1} = u_{i,j}^{n} + \Delta t \cdot \left[\nabla \cdot (q(x_i, y_j)\nabla u)\right]_{i,j}^{n+1}. \tag{3.8}$$

This equation is solved iteratively at each time step to obtain $u_{i,j}^{n+1}$.
Application of the Neumann boundary conditions $\frac{\partial u}{\partial n} = 0$, leads us to use a symmetry method at the boundary.
For example, at the limit $x = 0$, the condition becomes:

$$\frac{u_{1,j}^{n+1} - u_{-1,j}^{n+1}}{2h_x} = 0 \quad \Rightarrow \quad u_{-1,j}^{n+1} = u_{1,j}^{n+1}. \tag{3.9}$$

Thus, we impose:

$$u_{0,j}^{n+1} = u_{1,j}^{n+1}. \tag{3.10}$$

Similarly, for the other boundaries, we apply:

$$u_{0,j}^{n+1} = u_{1,j}^{n+1}, \quad u_{N_x+1,j}^{n+1} = u_{N_x-1,j}^{n+1}, \tag{3.11}$$

and analogously for the y-direction.

This symmetric extension ensures that the Neumann boundary conditions are properly enforced in the numerical scheme.

3.2. Algorithm

The discretization of the proposed model can be summarized by the following algorithm 1, which summarizes the various steps involved in the numerical solution of the anisotropic diffusion equation with controlled diffusion coefficient. The algorithm features an iterative evolution to restore the noisy image while preserving essential structures, such as contours, thanks to an adaptive adjustment of the diffusion term.

Algorithm 1 Explicit sheme of the proposed controlled diffusion model

Initialization :
Load noisy image f, size $m \times n$
Select parameters Δt, T, α, ϵ
Define $N = \frac{T}{\Delta t}$, $q^0 = 1$, $p^0 = 0$, $u^0 = f$
Calculate the initial gradient ∇f et $\partial R/\partial q$
for $k = 0$ to $N - 1$ **do**
Calculate the Laplacian $L^k = \Delta u^k$
Calculate the gradient ∇p^k
Calculate $\mathrm{div}(q^k \nabla p^k)$
Update :

$$p^{k+1} = p^k + \Delta t \left(\mathrm{div}(q^k \nabla p^k) + u^k - f + \alpha q^k L^k\right)$$

Calculate the gradient of u^k and p^k
Update :

$$q^{k+1} = q^k - \Delta t \cdot \frac{\nabla u^k \cdot \nabla p^k}{\alpha(|\nabla u^k|^2 + \epsilon)}$$

Calculate divergence $\mathrm{div}(\nabla p^{k+1})$
Update :

$$u^{k+1} = u^k + \Delta t \left(-\mathrm{div}(\nabla p^{k+1}) + u^k - f + (q^{k+1})^2 L^k\right)$$

Apply homogeneous Neumann conditions to edges.
end for
Exit : restored image u

Remark:
It may be noted that the proposed algorithm is based on explicit time discretization, which allows simple numerical implementations, but on the other hand imposes a stability constraint on the time step δt. More specifically, the joint iteration of state u, adjoint multiplier p and control function q in a fully decoupled scheme may cause error amplification if the stopping criterion or CFL conditions are not met. A future solution could be to switch to semi-implicit or implicit discretization, which would stabilize iteration, as envisaged, for example, by Weickert (1998) in the context of anisotropic diffusion, or Aubert and Kornprobst (2006) for variational regularization.

4. Numerical results

In this section, we present numerical results with the aim of juxtaposing the effectiveness of our technique with that of traditional models such as the heat equation and the Perona-Malik model. Three standard images were tested after being degraded by additive Gaussian noise of zero mean and various variances. Quantitative evaluation is based on three parameters: peak signal-to-noise ratio (PSNR), mean square error (MSE) and signal-to-noise ratio (SNR). Their expressions are as follow:

$$\mathrm{MSE} = \frac{1}{N} \sum_{i=1}^{N} (u_i - \hat{u}_i)^2 , \tag{4.1}$$

$$\mathrm{PSNR} = 10 \log_{10} \left(\frac{(\mathrm{MAX}_u)^2}{\mathrm{MSE}} \right) , \tag{4.2}$$

$$\mathrm{SNR} = 10\log_{10}\left(\frac{\sum_{i=1}^{N} u_i^2}{\sum_{i=1}^{N}(u_i - \hat{u}_i)^2}\right), \tag{4.3}$$

Table 1 summarizes the performance obtained for each image and each degree of noise.

Table 1: Comparison of different models with 3 different images using the PSNR, MSE and SNR values.

Image	**Variance** $[\sigma^2]$	**Noisy**	**Heat equation**	**Perona-Malik**	**Our approach**
Cameramen	$\sigma^2 = 0.001$	PSNR=30.12 MSE=24.55 SNR=24.54	PSNR=24.29 MSE=18.59 SNR=18.71	PSNR=31.12 MSE=24.55 SNR=24.54	PSNR=**32.9164** MSE=**27.3051** SNR=**25.6799**
	$\sigma^2 = 0.003$	PSNR=25.48 MSE=19.94 SNR=19.89	PSNR=24.17 MSE=18.47 SNR=18.59	PSNR=25.48 MSE=19.94 SNR=19.89	PSNR=**30.6847** MSE=**25.0858** SNR=**22.5749**
	$\sigma^2 = 0.005$	PSNR=23.30 MSE=17.80 SNR=17.72	PSNR=24.03 MSE=18.34 SNR=18.45	PSNR=23.30 MSE=17.80 SNR=17.72	PSNR=**29.2738** MSE=**23.6886** SNR=**20.7447**
Lena	$\sigma^2 = 0.001$	PSNR=29.99 MSE=24.35 SNR=24.34	PSNR=30.57 MSE=24.87 SNR=24.91	PSNR=29.99 MSE=24.35 SNR=24.34	PSNR=**36.2965** MSE=**30.6383** SNR=**27.5471**
	$\sigma^2 = 0.003$	PSNR=25.22 MSE=19.61 SNR=19.56	PSNR=30.16 MSE=24.46 SNR=24.50	PSNR=25.22 MSE=19.61 SNR=19.56	PSNR=**32.1988** MSE=**26.5509** SNR=**23.0964**
	$\sigma^2 = 0.005$	PSNR=23.02 MSE=17.44 SNR=17.36	PSNR=29.78 MSE=240.9 SNR=24.12	PSNR=23.02 MSE=17.44 SNR=17.36	PSNR=**30.1818** MSE=**24.5509** SNR=**21.1006**
Eight	$\sigma^2 = 0.001$	PSNR=30.02 MSE=28.14 SNR=28.13	PSNR=28.98 MSE=27.07 SNR=27.09	PSNR=30.02 MSE=28.14 SNR=28.13	PSNR=**34.8863** MSE=**32.9961** SNR=**30.684**
	$\sigma^2 = 0.003$	PSNR=25.37 MSE=23.49 SNR=23.48	PSNR=28.70 MSE=26.79 SNR=26.82	PSNR=25.37 MSE=23.49 SNR=23.48	PSNR=**31.7784** MSE=**29.8876** SNR=**26.7816**
	$\sigma^2 = 0.005$	PSNR=23.38 MSE=21.51 SNR=21.49	PSNR=28.44 MSE=26.52 SNR=26.56	PSNR=23.38 MSE=21.51 SNR=21.49	PSNR=**30.0523** MSE=**28.1505** SNR=**24.8861**

This table 1 illustrates the comparison of the restoration quality of three images, assessed by PSNR, MSE and SNR, as a function of various levels of Gaussian noise. It is clear that our method offers better performance than traditional diffusion models, particularly in terms of PSNR values, which reflect a more faithful reconstruction.

In Figures 1, 2 and 3, we present results for denoising a series of test images. The images have been degraded by an additive Gaussian noise of standard deviation of $\sigma^2 = 0.001,\ 0.003,\ 0.005$.

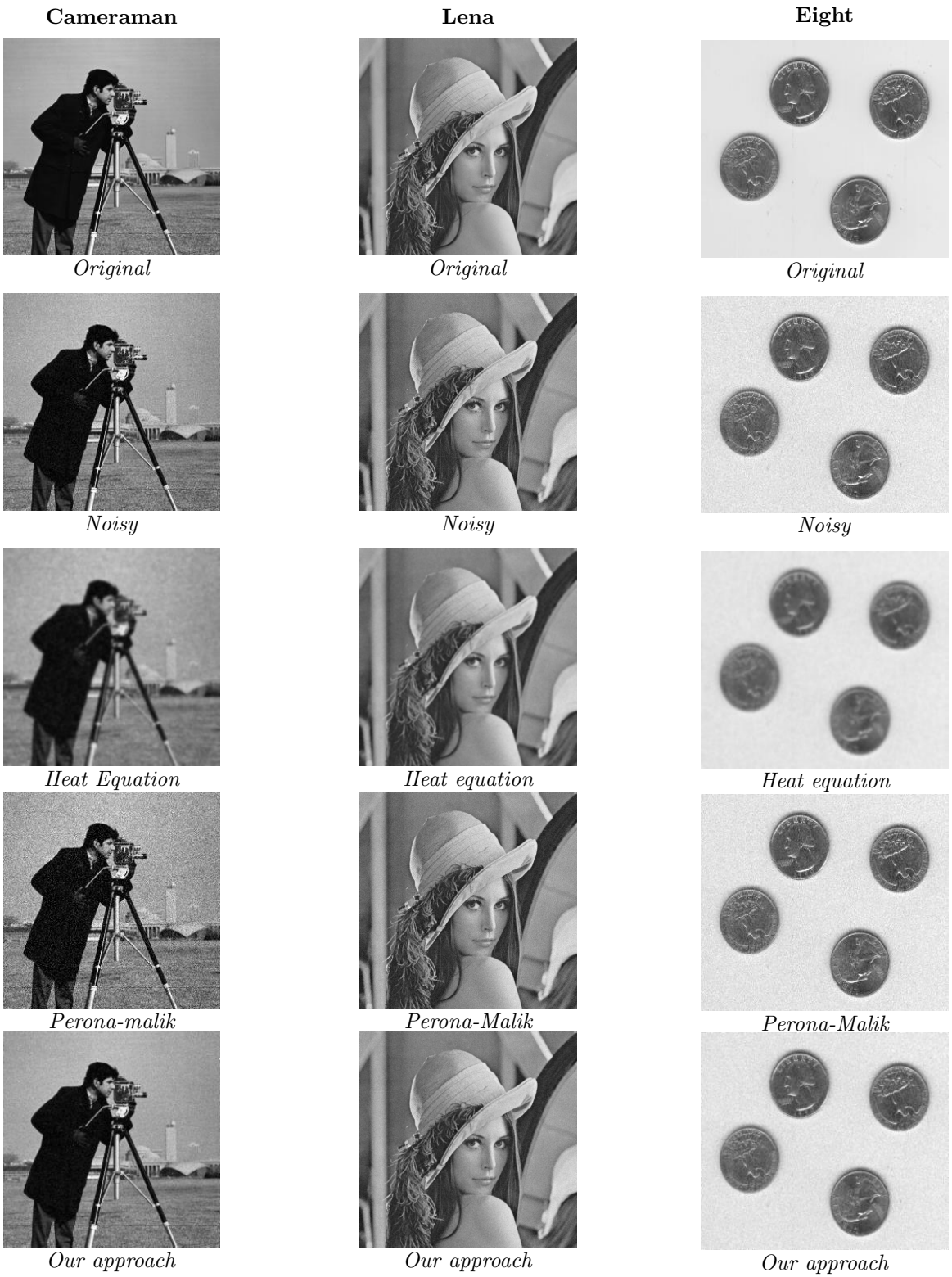

Figure 1: Comparison of original, noisy, and denoised images for $\sigma^2 = 0.001$.

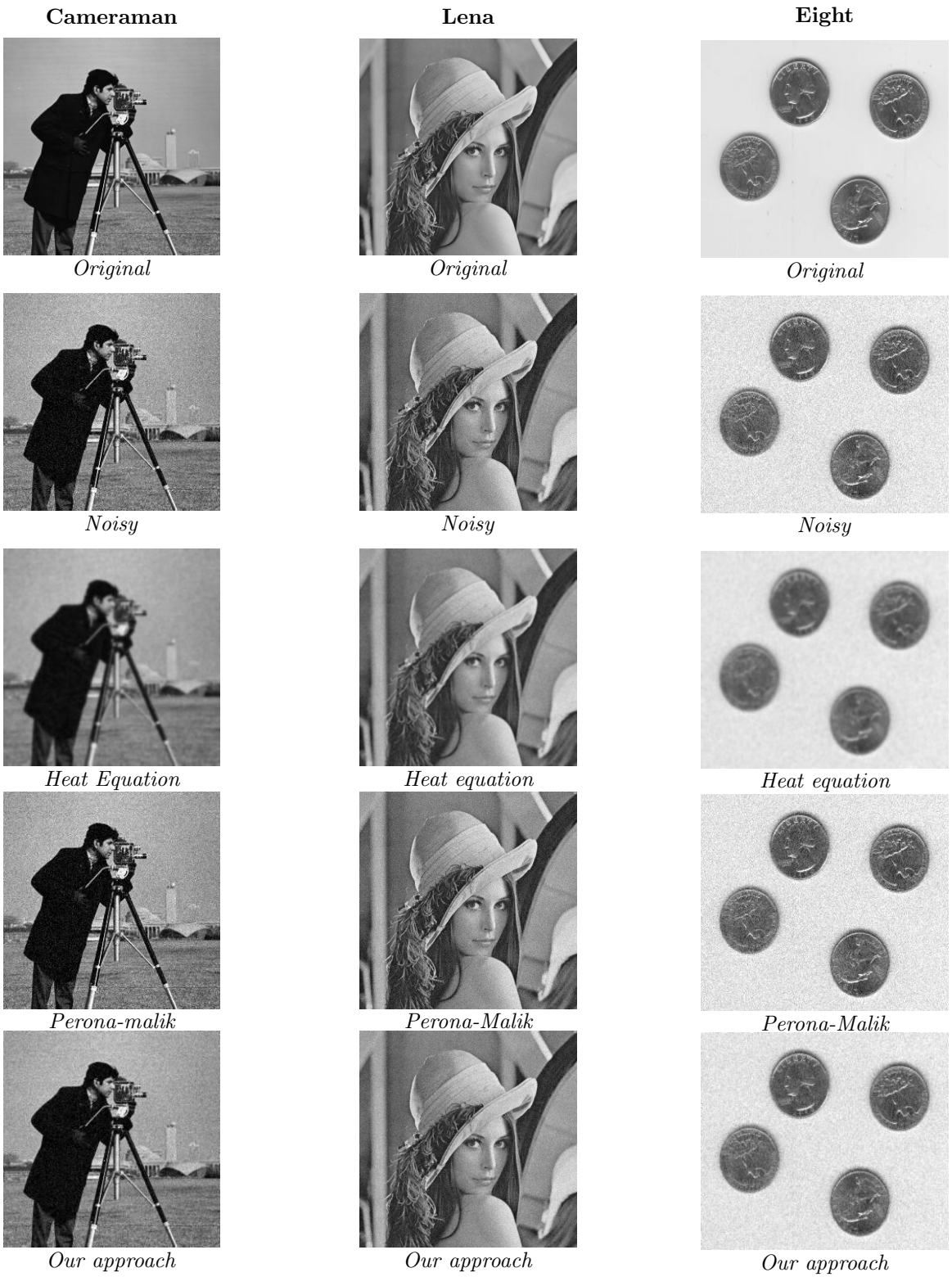

Figure 2: Comparison of original, noisy, and denoised images for $\sigma^2 = 0.003$.

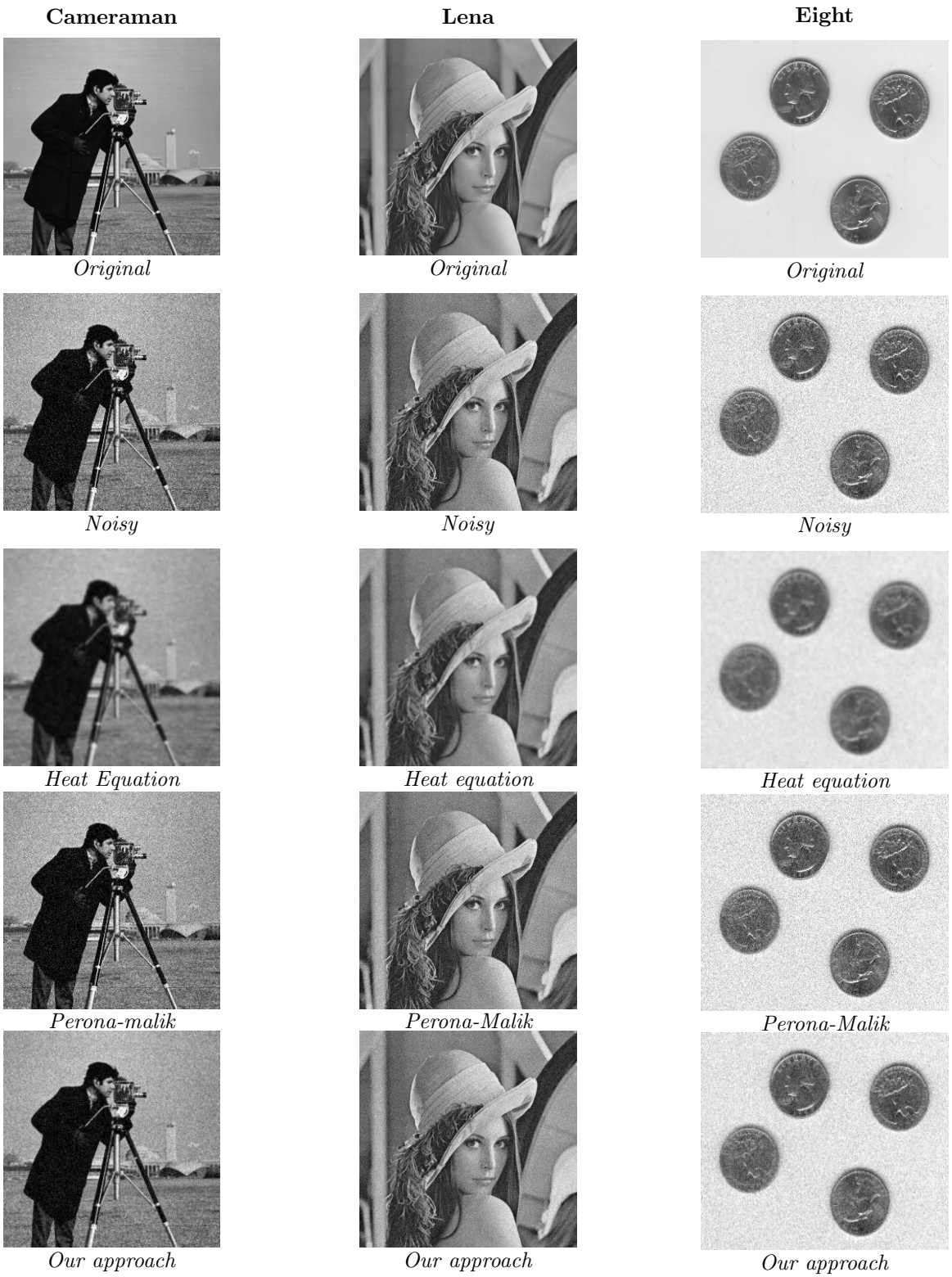

Figure 3: Comparison of original, noisy, and denoised images for $\sigma^2 = 0.005$.

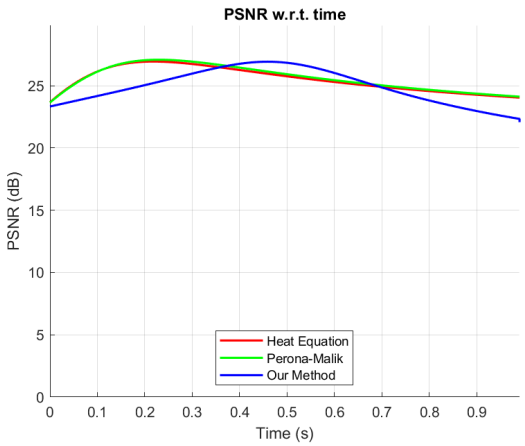

Figure 4: The quantitative results of the PSNR evolution over time for Cameraman image while $\sigma^2 = 0.005$.

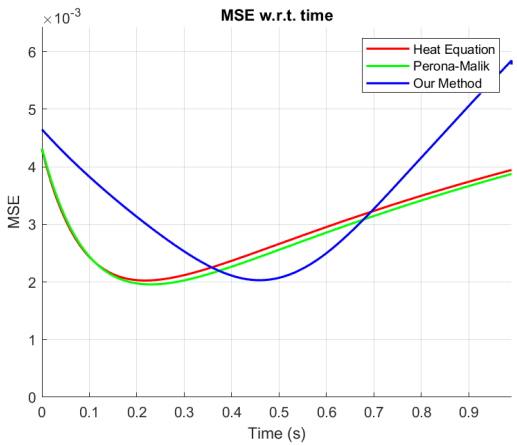

Figure 5: The quantitative results of the MSE evolution over time for Cameraman image while $\sigma^2 = 0.005$.

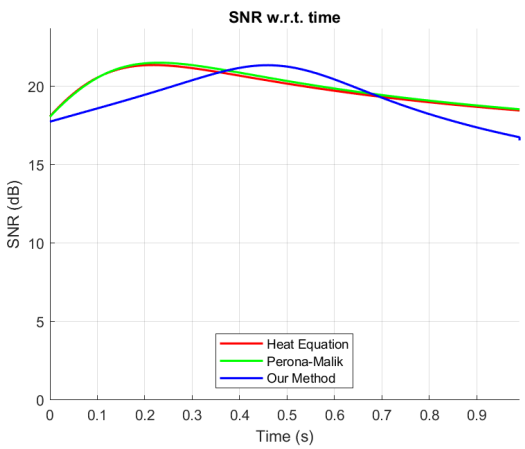

Figure 6: The quantitative results of the SNR evolution over time for Cameraman image while $\sigma^2 = 0.005$.

As previously discussed, the proposed method is built upon the concept of controlled diffusion, aiming to suppress noise while preserving the most relevant image features, particularly edges and contours, as illustrated in Figures 1–3. Unlike uniform diffusion methods—such as the heat equation—which apply the same smoothing strength across the entire image and consequently blur details that should be preserved, the controlled diffusion strategy adapts the diffusion intensity locally through a spatially dependent control function. In practical terms, the noisy image evolves according to a simulated process that selectively smooths flat regions, where noise dominates, while significantly limiting diffusion near contours and fine structures, thereby safeguarding visual quality. The spatial control mechanism is automatically derived from local image variations, guided by the detection of high-contrast regions. The resulting restored image represents an optimal balance between noise reduction and preservation of essential visual details. When compared with established models, such as Perona–Malik diffusion or the classical heat equation, the proposed framework exhibits greater adaptability to diverse structural patterns, leading to enhanced preservation of tonal and structural details. Quantitative evaluations—measured by PSNR, MSE, and SNR—confirm the superiority of our approach, as shown in Figures 4, 5, and 6.

5. Conclusion

The proposed image denoising framework relies on a regulated diffusion process designed to suppress noise while preserving essential image characteristics, particularly edges and contours that are critical for human perception and subsequent image analysis. Traditional approaches, such as the linear heat equation or the Perona-Malik anisotropic diffusion, typically employ constant or fixed diffusivity functions. While effective to some extent, these methods often cause undesirable blurring of important details or generate visual artifacts. In contrast, the present method incorporates a spatially adaptive control parameter that modulates the diffusion strength according to the local image structure. This adaptability enables selective smoothing: homogeneous regions are efficiently denoised, whereas high-gradient areas retain their sharpness. Both quantitative indicators and qualitative evaluations of visual fidelity demonstrate that the proposed scheme consistently outperforms conventional models in extensive tests on standard benchmark datasets. By embedding this spatially variable control mechanism, the diffusion process becomes more responsive to the underlying image content, ensuring that the restoration process aligns closely with the scene's intrinsic features. Beyond Gaussian noise suppression, the model shows promise for extension to other degradation types, including impulsive and multiplicative noise. Furthermore, it offers potential for integration into hybrid frameworks that merge PDE-based controlled diffusion with variational formulations or modern data-driven methods, such as machine learning, thereby paving the way for more robust and versatile image restoration strategies.

References

1. G. Aubert and P. Kornprobst, *Mathematical Problems in Image Processing: Partial Differential Equations and the Calculus of Variations*, 2nd ed., vol. 147, Springer, New York, 2006.
2. R. C. Gonzalez and R. E. Woods, *Digital Image Processing*, 4th ed., Pearson, 2018.
3. K. Zhang, W. Zuo, Y. Chen, D. Meng, and L. Zhang, "Beyond a Gaussian denoiser: Residual learning of deep CNN for image denoising," *IEEE Trans. Image Process.*, vol. 26, no. 7, pp. 3142–3155, 2017.
4. S. W. Zamir et al., "Restormer: Efficient Transformer for High-Resolution Image Restoration," in *Proc. IEEE/CVF Conf. Computer Vision and Pattern Recognition (CVPR)*, 2022, pp. 5728–5739.
5. A. Charkaoui, A. Ben-Loghfyry, *A class of nonlinear parabolic PDEs with variable growth structure applied to multi-frame MRI super-resolution*, Nonlinear Analysis: Real World Applications, 83(2025), p.104259.
6. A. Charkaoui, A. Ben-Loghfyry, *A novel multi-frame image super-resolution model based on regularized nonlinear diffusion with Caputo time fractional derivative*, Communications in Nonlinear Science and Numerical Simulation, 139(2024), p.108280.
7. A. Chambolle, "An algorithm for total variation minimization and applications," *Journal of Mathematical Imaging and Vision*, vol. 20, no. 1–2, pp. 89–97, 2004.
8. A. Ben-Loghfyry, A. Hakim, *A novel robust fractional-time anisotropic diffusion for multi-frame image super-resolution*, Advances in Computational Mathematics, 49(6), p.79.
9. R. Addouch, N. Moussaid, O. Gouasnouane and A. Ben-Loghfyry, *Total fractional-order variation and bilateral filter for image denoising*, Mathematical modeling and computing, (11, Num. 3) (2024), pp.642-653.

10. A. Ben-Loghfyry, *A fractional-time PDE-constrained parameter identification for inverse image noise removal problem*, Journal of the Franklin Institute, 362(2), 2025, p.107443.

11. A. Charkaoui, A. Ben-Loghfyry and S. Zeng, *A novel parabolic model driven by double phase flux operator with variable exponents: Application to image decomposition and denoising*, Computers & Mathematics with Applications, 174(2024), pp.97-141.

12. A. Charkaoui, A. Ben-Loghfyry, *Anisotropic equation based on fractional diffusion tensor for image noise removal*, Mathematical Methods in the Applied Sciences, 47(12), 2024, pp.9600-9620.

13. O. Gouasnouane, N. Moussaid, S. Boujena and K. Kabli, *A nonlinear fractional partial differential equation for image inpainting*, Math. Model. Comput, 9(2022), pp.536-546.

14. A. Ben-loghfyry and A. Hakim, *Caputo fractional-time of a modified Cahn-Hilliard equation for the inpainting of binary images*, Journal of Mathematical Modeling, 11(2), 2023, pp.357-373.

15. F.Y. Shih, *Image processing and pattern recognition: fundamentals and techniques*, 2010, John Wiley & Sons.

16. M. Kaur and V. Kumar,*A comprehensive review on image encryption techniques*, Archives of Computational Methods in Engineering, 27(1), 2020, pp.15-43.

17. A. Krull, T.-O. Buchholz, and F. Jug, "Noise2Void – Learning denoising from single noisy images," in *Proc. IEEE/CVF Conf. Computer Vision and Pattern Recognition (CVPR)*, 2019, pp. 2129–2137.

18. A. Buades, B. Coll, and J.-M. Morel, "A non-local algorithm for image denoising," in *Proc. IEEE Conf. Computer Vision and Pattern Recognition (CVPR)*, 2005, pp. 60–65.

19. L. I. Rudin, S. Osher, and E. Fatemi, "Nonlinear total variation based noise removal algorithms," *Physica D: Nonlinear Phenomena*, vol. 60, no. 1–4, pp. 259–268, 1992.

20. C. Tian, L. Fei, W. Zheng, Y. Xu, and Z. Luo, "Deep learning on image denoising: An overview," *Neural Networks*, vol. 131, pp. 251–275, 2020.

21. P. Perona and J. Malik, "Scale-space and edge detection using anisotropic diffusion," *IEEE Trans. Pattern Anal. Mach. Intell.*, vol. 12, no. 7, pp. 629–639, 1990.

22. J. Weickert, *Anisotropic Diffusion in Image Processing*, Teubner, Stuttgart, 1998.

23. G. Gilboa and S. Osher, "Nonlocal operators with applications to image processing," *Multiscale Modeling & Simulation*, vol. 7, no. 3, pp. 1005–1028, 2008.

24. A. N. Tikhonov and V. Y. Arsenin, *Solutions of Ill-posed Problems*, Winston and Sons, Washington, DC, 1977.

25. J.-L. Lions, *Optimal Control of Systems Governed by Partial Differential Equations*, Springer-Verlag, 1971.

26. S. Bonettini, M. Prato, and S. Rebegoldi, "A scaled gradient projection method for constrained image deblurring," *Inverse Problems*, vol. 34, no. 1, 2018.

27. J.-L. Lions, *Quelques méthodes de résolution des problèmes aux limites non linéaires*, Dunod, Paris, 1969.

28. O. A. Ladyzhenskaya, *The Boundary Value Problems of Mathematical Physics*, Springer, New York, 1985.

29. I. Ekeland and R. Temam, *Convex Analysis and Variational Problems*, SIAM, Philadelphia, 1999.

30. E. Casas, "Control of an elliptic problem with pointwise state constraints," *SIAM Journal on Control and Optimization*, vol. 24, no. 6, pp. 1309–1318, 1986.

31. M. Hinze, R. Pinnau, M. Ulbrich, and S. Ulbrich, *Optimization with PDE Constraints*, Springer, Heidelberg, 2009.

32. J. Weickert, *Anisotropic Diffusion in Image Processing*, Teubner, Stuttgart, 2002.

33. G. D. Smith, *Numerical Solution of Partial Differential Equations: Finite Difference Methods*, 3rd ed., Oxford University Press, Oxford, 1985.

34. L. N. Trefethen, *Spectral Methods in MATLAB*, Software, Environments, and Tools, Vol. 10, SIAM, Philadelphia, 2000.

35. K. Zhang, W. Zuo, and L. Zhang, "FFDNet: Toward a fast and flexible solution for CNN-based image denoising," *IEEE Trans. Image Process.*, vol. 27, no. 9, pp. 4608–4622, 2018.

[1] *LMCA, FSTM of Mohammedia, Hassan II University of Casablanca, Morocco*

[2] *MSPASI, FSTM of Mohammedia, Hassan II University of Casablanca, Morocco*

E-mail address: anouar.benloghfyry@univh2c.ma